# Multiple Bifurcation Types and the Linear Dynamics of Ion Sputtered Surfaces

# Multiple Bifurcation Types and the Linear Dynamics of Ion Sputtered Surfaces

Charbel S. Madi,[1] Benny Davidovitch,[2] H. Bola George,[1] Scott A. Norris,[1] Michael P. Brenner,[1] and Michael J. Aziz[1]
[1]*Harvard School of Engineering and Applied Sciences, Cambridge Massachusetts 02138, USA*
[2]*Department of Physics, University of Massachusetts, Amherst Massachusetts 01002, USA*
(Received 3 December 2007; published 9 December 2008)

We study the patterns formed on ion sputtered Si surfaces as a function of ion energy and incidence angle, and identify a region in parameter space where the flat surface is stable. The boundaries between the stable and pattern-forming regions represent mathematical bifurcations. Our data set exhibits at least two different bifurcation types. We discuss the constraints imposed by these observations on the correct model of long wavelength dynamics of ion sputtered surfaces.

DOI: 10.1103/PhysRevLett.101.246102 PACS numbers: 68.49.Sf, 81.16.Rf, 81.65.Cf

Uniform ion beam sputter erosion of a solid surface often causes a spontaneously arising pattern in the surface topography that can take the form of corrugations or arrays of dots [1]. Periodic self-organized patterns with wavelength as small as 7 nm [2] have stimulated interest in this method as a means of sublithographic nanofabrication [3]. The classical linear stability theory of Bradley and Harper (BH) [4] attributes the pattern to a competition between a destabilizing (roughening) effect in which the erosion rate is enhanced at regions of high concave curvature and the stabilizing (smoothening) effect of surface diffusion. The BH theory explains several experimental observations, most notably the widespread observation of ''ripple rotation'': with increasing tilt from normal incidence, first the appearance of ''parallel-mode ripples'' (wave vector parallel to the projected ion beam) and then a transition to ''perpendicular-mode ripples'' (wave vector perpendicular to the ion beam). However, serious contradictions have recently emerged, related both to predictions of instabilities and amplification rates not seen experimentally, as well as to incorrect prediction of patterns in the nonlinear regime [1,5]. Resolving these inconsistencies is crucial for developing a theoretical framework for even qualitatively predicting evolving surface patterns, and is thus of critical importance for learning how to control and manipulate the surface patterns by ion irradiation. To this end, particular attention is paid to monatomic systems possessing surfaces that are amorphous under ion bombardment, thereby minimizing potentially confounding effects of disproportionation and crystallographic singularities.

In this Letter we focus on the disagreement between the linear stability analysis of BH, which predicts that a flat, uniformly irradiated surface is always unstable, and recent experiments documenting regimes of two control parameters—incident angle $\theta$ and ion energy $E$—where the flat surface is stable. Sharp boundaries between stable and unstable regimes in control parameter space are known as *bifurcations*. Nonequilibrium pattern formation theory predicts that, for any mechanism, near bifurcations pattern features are universal, depending only on general characteristics of the dynamics, such as its symmetries, degree of criticality (i.e., whether the amplitude vanishes or not), and whether the characteristic length scale vanishes, diverges, or remains finite at bifurcation [6]. Characterizing bifurcation type can thus place strong constraints on underlying physical models. Motivated by this insight, we carried out careful characterization of patterns around bifurcation points by varying both incidence angle and ion beam energy. Our major finding is that a single, monatomic, isotropic system exhibits two different types of supercritical bifurcations as incidence angle and ion energy are varied: a bifurcation of type I, characterized by constant wavelength, and another bifurcation, of type II, characterized by diverging wavelength. This observation, supplemented by analysis of evolving patterns near and away from bifurcations, leads us to point out the inadequacy of all existing models and to impose strong constraints on the dominant physical mechanisms.

We performed argon ion ($Ar^+$) irradiation experiments on 1 $cm^2$ Si(001) square samples ($p$ type, 1–10 $\Omega$ cm) in an ultrahigh vacuum chamber (base pressure $7 \times 10^{-11}$ torr at room temperature) with the projected ion beam direction along the [110] crystallographic direction. The argon ions were generated using a 3-cm rf source with graphite accelerating grids [7]. To vary the incidence angle $\theta$, samples were fixed, using melted indium, onto graphite wedges of various angles which were shielded everywhere from the ion beam by Si wafer shields. Thus, only silicon is exposed to the direct ion beam [8] and contamination-induced dynamics [9] is suppressed. The ion flux from the source was 0.57 mA $cm^{-2}$ in the plane perpendicular to the ion beam. The beam divergence was roughly 4.5° and the distance to the target was approximately 15 cm. The surface should become amorphous [10] very quickly, after a fluence of the order $10^{14}$ ions $cm^{-2}$ [11]. Patterns for $\theta < 25°$ ($\theta > 45°$) are first observed at a fluence of $\sim 2 \times 10^{18}$ ($1 \times 10^{17}$) $cm^{-2}$. Pattern amplification drops below exponential, without much change in lateral length scale [12], at a fluence of $\sim 5 \times 10^{18}$ ($5 \times 10^{17}$) $cm^{-2}$.

After irradiation, atomic force microscopy (AFM) images were obtained from a Digital Instruments Nanoscope D3100 AFM in tapping mode. Figure 1 shows the existence

 

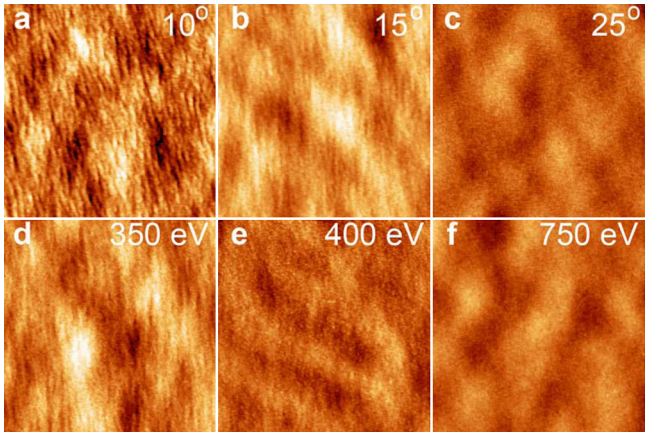


FIG. 1 (color online). (a)–(c) Effect of incidence angle on surface morphology following irradiation with 250 eV $Ar^+$ at ambient temperature. (d)–(f) Effect of ion energy on surface morphology of Si(001) following irradiation at 10° off-normal incidence angle and ambient temperature. In all cases, the substrate is at ambient temperature and the ion fluence is $3.8 \times 10^{18}$ $Ar^+$ $cm^{-2}$ (18 min), the projected ion beam runs from the bottom of the page to the top, the AFM topograph scan size is 2 $\mu$m × 2 $\mu$m, and the vertical scale is 2 nm.

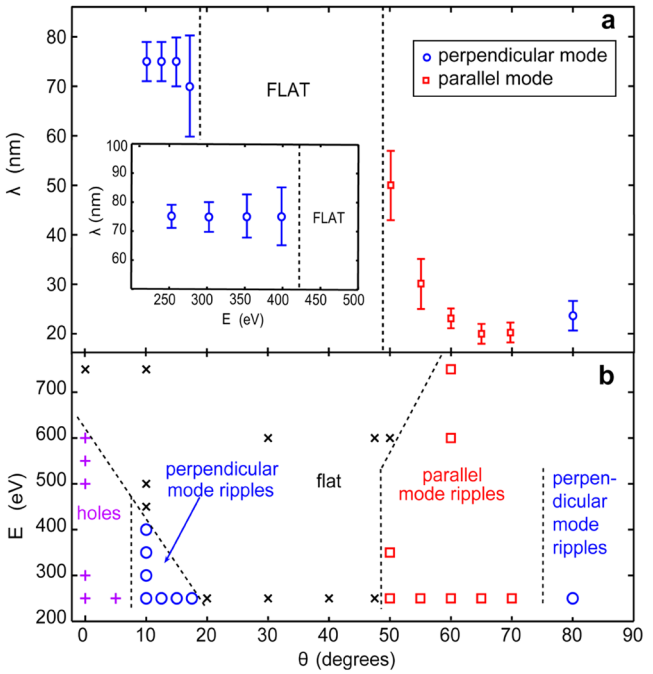


FIG. 2 (color online). (a) Dependence of instability wavelength on ion incidence angle during 250 eV $Ar^+$ irradiation. Circles: perpendicular mode; squares: parallel mode. Inset: Perpendicular-mode wavelength versus $E$ at $\theta = 10°$. (b) Phase diagram for control parameters $\theta$ and $E$. ×: flat; +: holes; circles: perpendicular-mode ripples; squares: parallel-mode ripples. Fluence is $3.8 \times 10^{18}$ $Ar^+$ $cm^{-2}$ except for ripples at $\theta \geq 50°$, where fluence is $3.2 \times 10^{17}$ $Ar^+$ $cm^{-2}$.

of a regime of control parameters for which a flat surface is stable under uniform ion sputter erosion. We demonstrated true stability by taking samples roughened by irradiating at 250 eV and 10°, and observing decay at all wave vectors upon further irradiation at 500 eV and 10° (Fig. 4.6 of [12]).

As the control parameter ($\theta$ or $E$) traverses a critical value, we see a transition from a rippling instability to a stable flat surface. To characterize this transition, we measured the rms roughness and wavelength of the evolving pattern as the control parameters approach the bifurcation points. Figure 2(a) reports the dependence of wavelength on $\theta$ and $E$ as the bifurcation points are traversed. Two central features are evident. As the low angle transition is approached, the wavelength remains practically constant [13]. At the high angle transition, the wavelength grows rapidly, apparently indicating divergence [14]. Figure 2(b) shows a phase diagram of the patterns observed in the linear regime as a function of $\theta$ and $E$: several qualitative features including an isotropic array of holes at normal incidence agree with [15].

Figure 3 focuses on the pattern amplification near the bifurcation points. Figure 3(a) shows that the amplification rate varies quadratically with deviation from the high-$\theta$ bifurcation point. The inset shows the time dependence of the amplitude for $\theta$ approaching this point: exponential growth at early time is consistent with the linear regime of pattern amplification. Figure 3(b) shows the wavelength versus misorientation. Figures 3(c) and 3(d) show the amplification rate versus control parameter near the low-$\theta$ bifurcation point. The differing power laws for the lines superposed on the low- (high-)$\theta$ bifurcations are those expected for a finite (infinite) wavelength bifurcation [6].

The continuously vanishing amplification rate indicates that all observed bifurcation points are supercritical. In the vicinity of supercritical bifurcations, pattern formation can be described by universal equations whose form depends only on general symmetries of the underlying dynamics and on the growth rate of the most unstable modes [6]. Therefore, a correct theoretical description of the patterns must agree with the global sequence of the experimentally identified bifurcations.

Theories of sputter erosion predict the evolution of a surface height profile $h(x; y; t)$. By assuming that the average response of the surface to the impact of a single ion is characterized by a cavity derived from Sigmund's Gaussian ellipsoid collision cascade model [16], BH found the linear surface dynamics on length and time scales much larger than those typical of the atomic response (1 nm, $10^{-10}$ sec , respectively):

$$\frac{\partial h}{\partial t} = -I + \{S_x \partial_{xx} + S_y \partial_{yy} - B\nabla^4\}h, \qquad (1)$$

where $I(\theta)$ is the vertical erosion rate of a flat surface, $S_x(\theta)$ and $S_y(\theta)$ are its curvature coefficients, $\theta$ is the angle between the normal to the flat surface and the ion beam direction, and $B$ is a material parameter describing relaxation and containing the surface free energy and either the

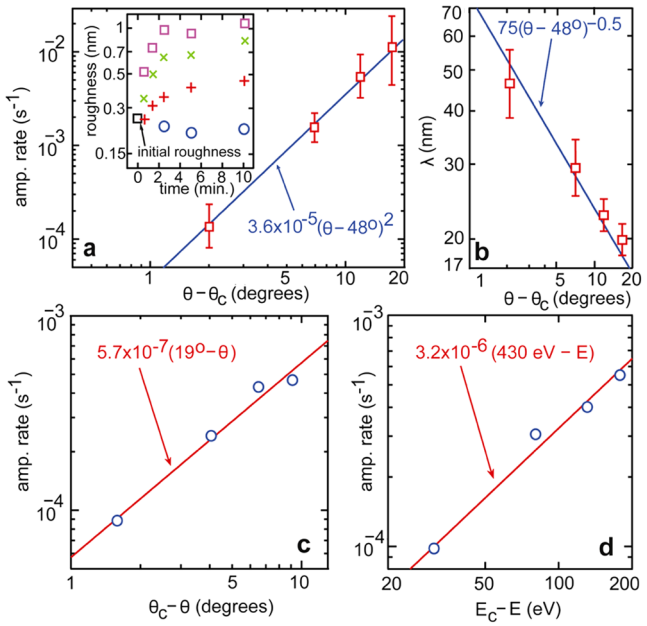


FIG. 3 (color online). Behavior near bifurcation points for (a), (b) high-$\theta$ and (c),(d) low-$\theta$ bifurcations. (a) Amplification rate versus misorientation for high-$\theta$ bifurcation. Inset: Pattern amplitude (reckoned as rms surface roughness) versus time. Squares: 65°; ×: 60°; +: 55°; circles: 50°. (b) Wavelength versus misorientation for high-$\theta$ bifurcation. (c) Amplification rate versus misorientation for low-$\theta$ bifurcation. (d) Amplification rate versus $E$ at $\theta = 10°$. In (a)–(c), $E = 250$ eV.

surface diffusivity or the viscosity of the ion-stimulated layer.

In the linear regime, this model and others we will discuss may be analyzed by considering the evolution of normal modes $h_{\mathbf{q}}(x, y, t) \propto e^{\omega_{\mathbf{q}} t}\cos(q_x x + q_y y)$ which, when inserted into Eq. (1), give the amplification rate $R_{\mathbf{q}}$:

$$R_{\mathbf{q}} \equiv \mathrm{Re}(\boldsymbol{\omega}_{\mathbf{q}}) = -S_x q_x^2 - S_y q_y^2 - B|\mathbf{q}|^4. \qquad (2)$$

The stability of a flat surface is determined by the sign of the maximum growth rate $\max\{R_{\mathbf{q}}\}$; $\max\{R_{\mathbf{q}}\} > 0$ ($< 0$) corresponds to instability (stability). In BH, $S_x$ and $S_y$ were deduced from Sigmund's Gaussian ellipsoid response, in which case $S_y < 0$ for all $\theta$ and $E$. Hence, for all values of $\theta$ and $E$, a flat surface is unstable for some wave vector perpendicular to the ion beam. Moreover, the BH theory predicts that for small $\theta$, $S_x < S_y < 0$, leading to dominance of parallel-mode ripples, whereas for large $\theta$ $S_y < S_x$, leading to dominance of perpendicular-mode ripples. The BH theory is thus contradicted firstly by the existence of a stable parameter regime, and secondly by our observations that perpendicular modes are the most unstable at small $\theta$.

Several modifications to the BH model have been proposed which allow stability for some range of incidence angles. Figure 4 illustrates three such models by highlighting their supercritical bifurcation points. The left-hand column of Fig. 4 considers a modification of BH [17] that replaces the BH curvature coefficients $S_x$; $S_y$ by effective coefficients $S_x^{\mathrm{eff}}$, $S_y^{\mathrm{eff}}$, whose parameter dependence contains regimes where both coefficients are positive, implying stability of flat surfaces. These can arise either from response functions to ion impact with shapes different than Gaussian ellipsoids or from nonerosive mass flow at the impact site [18]. Both of these modifications preserve the experimentally robust $\theta$ dependence of the sputter yield. With mass flow as the only modification to BH theory, $S_x^{\mathrm{eff}}$ and $S_y^{\mathrm{eff}}$ can both be positive at low angles, with a sign change in $S_x^{\mathrm{eff}}$ occurring at intermediate angles [17] causing a parallel-mode instability. Because the most unstable wave number $q_m = \sqrt{-S^{\mathrm{eff}}/2B}$, we have that $q_m \to 0$ as $S^{\mathrm{eff}}$ vanishes. Hence for these models the pattern wavelength diverges at the bifurcation point.

The middle column of Fig. 4 shows how this picture is modified by a damping term $-Kh$, where $K$ is a positive constant [19]. This results in a constant stabilizing contribution (i.e., $\propto -q^0$) to the amplification rate $R_{\mathbf{q}}$, causing the bifurcation point to occur at nonzero $S^{\mathrm{eff}}$ and $q$. We note that this term is offered as a proxy for a model of redeposition but has not been derived from more fundamental principles. Finally, the right-hand column of Fig. 4 shows the BH model augmented by a term caused from ion induced surface stress. This additional destabilizing term causes the Asaro-Tiller elastic energy-induced instability of solid surfaces [20,21], and may become relevant if sufficient stress accumulates during the ion irradiation process [22]. In this case the bifurcation occurs at finite $q$.

The terms described in Fig. 4 that cause bifurcations at nonzero $q$ require integral operators, whose range is much larger than the pattern wavelength. Although they are not

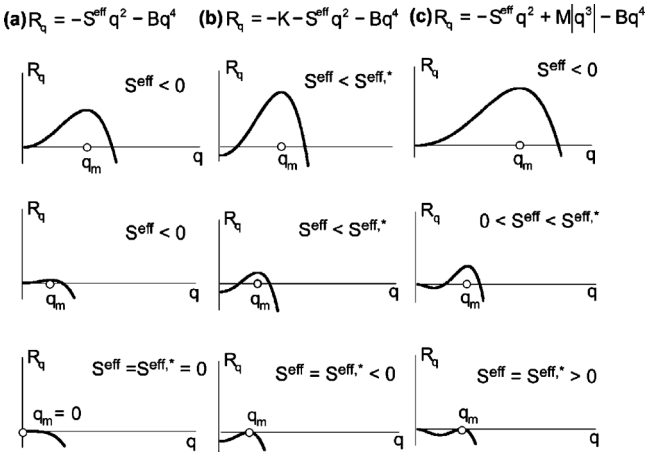


FIG. 4. Schematic plots depicting the transition from unstable to stable surface dynamics for three dispersion relations. (a) Left-hand column: generalized BH Eq. (1), where the transition occurs at $S^{\mathrm{eff},*} = 0$ with diverging wavelength. (b) Middle column: with Facsko nonlocal "damping term," transition occurs at $S^{\mathrm{eff},*} < 0$ with finite wavelength. (c) Right column: with Asaro-Tiller nonlocal elastic energy mechanism, transition occurs at $S^{\mathrm{eff},*} > 0$ with finite wavelength.

likely to be unique, they raise the intriguing possibility of the importance of nonlocal processes in addition to the local response of surfaces to ion impact.

Modification of only the coefficient of the quadratic term cannot reconcile theory and experiment, both because it retains a diverging wavelength at bifurcation [Fig. 4(a)] and because it predicts parallel mode at low angles contradicting our low angle experimental observations. The Asaro-Tiller mechanism gives rise to finite-wavelength bifurcations, which in principle may favor perpendicular mode at low angles due to higher stress in the perpendicular direction for off-normal incidence [23]. The main problem with this mechanism is that preliminary *in situ* stress measurements [23] indicate stresses less than 200 MPa for which the standard ($S^{\text{eff}} = 0$) model [21] predicts an instability wavelength 2 orders of magnitude larger than that observed. And allowing $S^{\text{eff}} \neq 0$ works only if $S^{\text{eff}} > 0$ [Fig. 4(c)], which predicts even longer wavelengths. Thus stress induced instability can work only if there is another (as yet unknown) mechanism for increasing the tenacity of the instability.

Another possible scenario posits that the shape of the single-impact crater function varies from Sigmund's Gaussian ellipsoid response so as to change the relative stability of perpendicular and parallel mode at low angle (so that $S_y^{\text{eff}} < S_x^{\text{eff}} < 0$), while reversing their stability $S_x^{\text{eff}} < S_y^{\text{eff}}$ ($S_x^{\text{eff}} < 0$) at higher angles. Although we do not have a specific example of such a crater function, previous work [17] demonstrates that small modifications to crater shapes easily change the relative stabilities of $S_x^{\text{eff}}$ and $S_y^{\text{eff}}$. In this form, the model would still predict diverging wavelengths at the bifurcation points. An additional process such as those discussed above would still have to be significant in the vicinity of the finite-wavelength bifurcation.

The experiment reported here, together with a careful analysis of the dynamics near bifurcation points, provides important constraints on the relevant physical processes in ion beam sputtering. Studies of pattern formation in other systems have shown that the physical processes identified this way are important even far from the bifurcation points. Our application of these tools has demonstrated that—in the linear regime for isotropic, elemental systems—at least one and quite possibly two additional physical effects beyond those in the classical theory are necessary to explain observed experimental results. A better understanding of the role of stress in the amorphous layer, a physical process leading to a nonlocal damping term, and the characterization of actual crater functions in physical experiment or molecular-dynamic simulation should be considered high research priorities. More generally, we suggest that pattern-forming analysis tools will provide more constraints on existing theories, as well as vetting new theories as they emerge.

C. S. M., H. B. G., and M. J. A. were supported by DE-FG02-06ER46335, and M. P. B. by NSF-0605031. B. D. acknowledges a travel grant by NWO. We thank W. Van Saarloos, B. Ziberi, and E. Chason for helpful discussions.

[1] W. L. Chan and E. Chason, J. Appl. Phys. **101**, 121301 (2007).
[2] Q. Wei *et al.*, Chem. Phys. Lett. **452**, 124 (2008).
[3] A. Cuenat *et al.*, Adv. Mater. **17**, 2845 (2005).
[4] R. M. Bradley and J. M. Harper, J. Vac. Sci. Technol. A **6**, 2390 (1988).
[5] B. Ziberi *et al.*, Phys. Rev. B **72**, 235310 (2005).
[6] M. C. Cross and P. C. Hohenberg, Rev. Mod. Phys. **65**, 851 (1993).
[7] Veeco, Fort Collins, CO.
[8] Energy dispersive x-ray spectrometry, x-ray photoelectron spectrometry, and a scanning tunneling electron microscopy map scan were employed to assess the surface impurity coverage of some of the Si samples after the completion of ion sputtering. The only elements that were evident were Si, O, Ar, and C, and the O and C signals from the ion beam sputtered samples were indistinguishable from those from a Si wafer taken directly out of the box.
[9] G. Ozaydin *et al.*, J. Vac. Sci. Technol. B **26**, 551 (2008).
[10] The amorphousness of our ion sputtered Si samples was assessed using cross-section TEM. The amorphous layer was about 3 nm thick in both the stable flat and unstable rippling surface. Furthermore, in a control experiment at 250 eV and 10°, no difference was found between pattern development on a crystalline Si wafer and on a wafer preamorphized with an 80 keV $Si^+$ implant to a dose of $10^{16}$ $cm^{-2}$ that resulted in an initial amorphous layer thickness of 192 nm.
[11] W. Bock, H. Gnaser, and H. Oechsner, Surf. Sci. **282**, 333 (1993).
[12] H. B. George, Ph.D. thesis, Harvard University, 2007.
[13] We find the same qualitative behavior—a transition to a flat surface between 280 °C and 300 °C—as the temperature $T$ is raised at 10° off-normal incidence with ion energy 250 eV. We do not dwell on this case, however, because complications may arise involving a potentially decreasing degree of amorphousness of the surface with increasing $T$. Likewise, R. Gago *et al.*, Phys. Rev. B **73**, 155414 (2006) reported no divergence in the dot spacing of saturated Si structures at normal incidence as the transition to flatness is approached with increasing $T$.
[14] Similar behavior was reported in sapphire by H. Zhou *et al.*, Phys. Rev. B **75**, 155416 (2007).
[15] B. Ziberi, Ph.D. thesis, University of Leipzig, 2006.
[16] P. Sigmund, J. Mater. Sci. **8**, 1545 (1973).
[17] B. Davidovitch, M. J. Aziz, and M. P. Brenner, Phys. Rev. B **76**, 205420 (2007).
[18] G. Carter and V. Vishnyakov, Phys. Rev. B **54**, 17 647 (1996); M. Moseler *et al.*, Science **309**, 1545 (2005).
[19] S. Facsko *et al.*, Phys. Rev. B **69**, 153412 (2004); S. Vogel and S. J. Linz, Europhys. Lett. **76**, 884 (2006).
[20] R. J. Asaro and W. A. Tiller, Metall. Trans. **3**, 1789 (1972).
[21] B. J. Spencer, P. W. Voorhees, and S. H. Davis, J. Appl. Phys. **73**, 4955 (1993).
[22] N. Kalyanasundaram *et al.*, Acta Mater. **54**, 483 (2006); G. Ozaydin *et al.* (unpublished).
[23] C. S. Madi, H. B. George, and M. J. Aziz (unpublished).